Simulation-Driven Virtual Prototyping of Smart Products

Jaehoon Kim, Smit Baua, Gopinath Gampala and Aniket Hegde
Altair Engineering, Troy, Mich.

Simulation-driven virtual prototyping is employed in the design of modern smart products to accelerate product development speed, ensure intrinsic product qualities and improve the decision-making process during development. It results in smart products that are more cost-effective with higher quality and reliability.
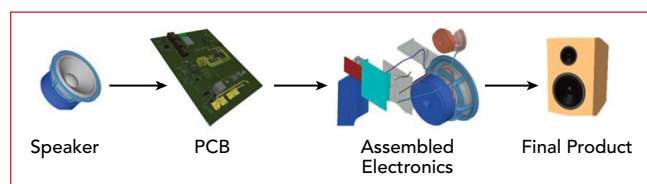
Over the past few decades, the wireless industry has experienced tremendous innovation and transformation, driven by the introduction of wireless communication standards such as 4G LTE, 5G, Bluetooth (BT) and Wi-Fi.[1] This, coupled with new rapid manufacturing techniques, requires advanced product design with complex multiphysics considerations. Competition in the consumer electronics market calls for designs that improve product performance while lowering development costs and reducing time to market. These challenges can be addressed by simulation-driven virtual prototyping to reduce physical testing.[2-4] Moreover, simulation-driven virtual prototyping can be employed in the design of modern smart products to accelerate product development speed,
ensure intrinsic product qualities and improve the decision-making process during development. Simulation-driven design is important for ensuring the completeness and timely market launch of smart products.
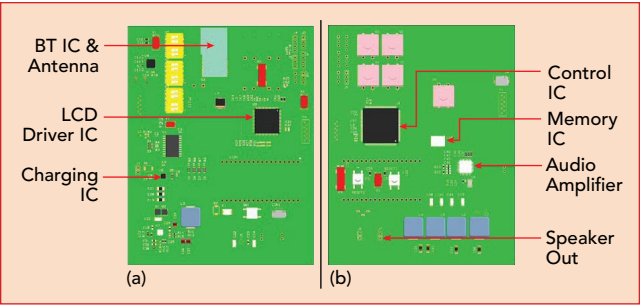
For example, **Figure 1** shows the product development process for a smart speaker assembly comprising a speaker component, printed circuit board (PCB), assembled electrical components and cabinet. A three-step simulation-driven virtual prototyping methodology was used in its development: 1) the design, verification and analysis of the PCB; 2) the design and integration of the BT antenna on the PCB inside the speaker cabinet; 3) a wireless communication performance evaluation of the smart speaker considering a neighboring wireless product.
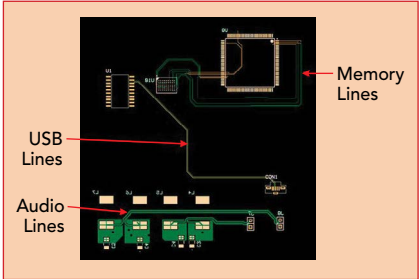
PCB DESIGN

The current generation of smart speakers receives audio signals wirelessly. One of the most popular RF standards supporting audio transmission to speakers is BT. A smart speaker includes a mostly BT wireless section, charging circuitry, audio amplifier for quality audio output, user display and the main controller with mem-

▲ Fig. 1 **Smart speaker components.**

Speaker   PCB   Assembled Electronics   Final Product

▲ **Fig. 2** Assembled PCB top (a) and bottom (b) views.

▲ **Fig. 3** PCB layout to be verified and analyzed.

ory that provides a reliable connection with the functional blocks. For a high-quality smart speaker, aspects such as audio signal quality, BT antenna performance and interference with other wireless signals must be considered.

Figure 2 shows the six-layer PCB with its electronic circuitry, which measures 106 × 137 × 0.7 mm thick. The board contains the audio amplifier; memory for storing wireless information such as pairing details, battery status and smart applications; USB connectivity for charging or diagnosing; charging and power supply circuitry; BT IC and antenna for wireless connectivity; and an LCD driver and display module. A microcontroller synchronizes the functionality of all the parts.

Although the ICs that define operational functionality are important, equally important are the other parts ensuring system reliability. The differential nets in audio lines, connectivity between the controller and the memory IC (i.e., the clock, address, command and data lines), differential data lines from the USB to the controller and the antenna for the BT module are crucial for meeting the quality and efficiency requirements.
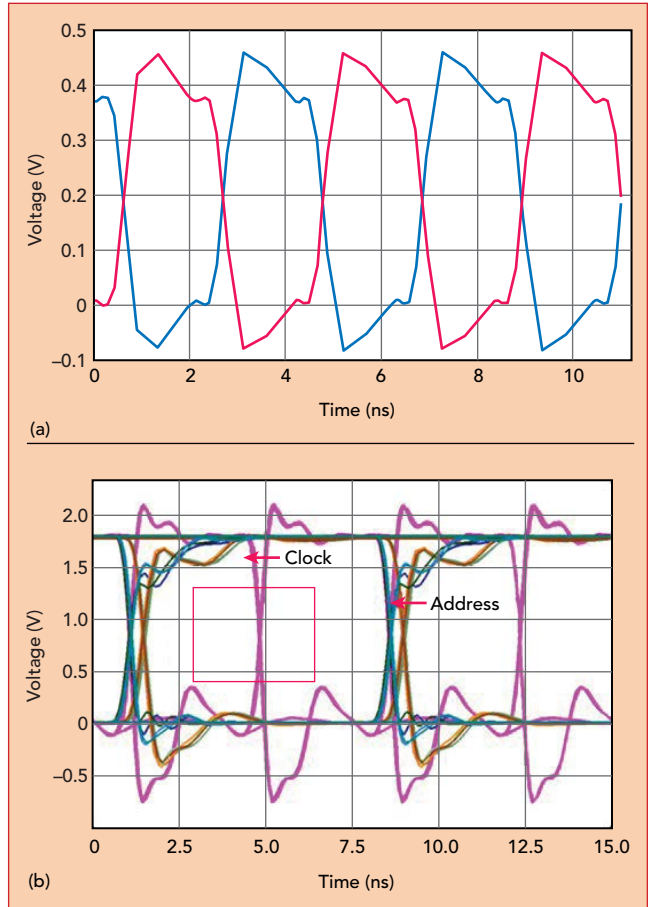
VERIFICATION AND ANALYSIS

Layout of the audio, USB and memory lines must be carefully de-signed for reliable operation, using verification and analysis methods to ensure design integrity. *Figure 3* shows the target layouts for verification and analysis of the differential audio and high speed lines (i.e., the USB interface and memory bus). To verify the differential audio line layout, a rule-based checker, Altair's PollEx PCB Verification for Design for Electrical Engineering, was used.[5] Signal integrity (SI) analysis was conducted to evaluate the layout of the high speed lines and the effects on transmitting and receiving digital signal waveforms and voltage/time margins. In addition to SI analysis, the thermal characteristics of the PCB were analyzed. Thermal analysis early in the design stage can identify excessive component temperatures and uneven board temperature.

The 0.5 mm wide differential audio lines were evaluated to assess the paired lines separation and coupling rate, because positive and negative lines must be tightly coupled within a specific distance. In *Table 1*, the separation criterion (center-to-center distance of 0.75 mm) was determined by adding the line width (0.5 mm) and the spacing between the lines (0.25 mm). The coupling rate criterion of bet-
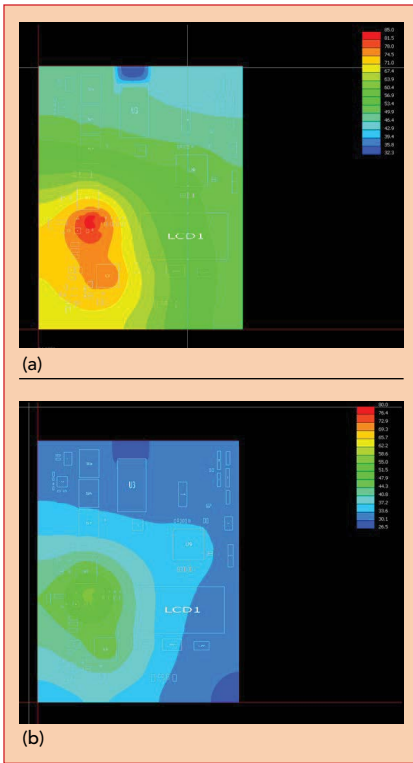
TABLE 1			
DIFFERENTIAL AUDIO LINE DFE RESULTS			
	Separation (mm)	*Coupling Rate (%)*	*Ground Shield Ratio (%)*
Criterion	0.75	> 80	> 80
Verified	0.893	76.6	Pass

▲ **Fig. 4** SI results: received signals at USB lines (a) and eye diagram for the clock and address lines of the memory bus (b).
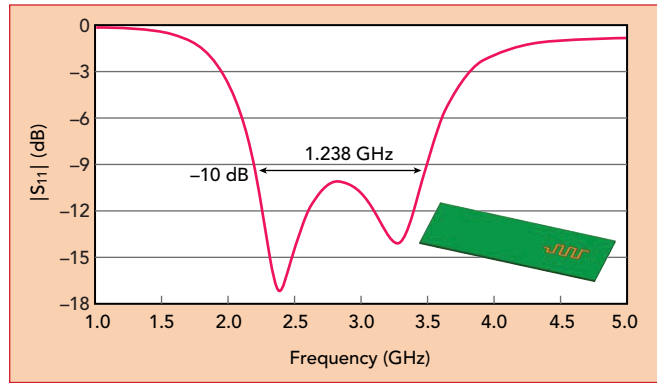
ter than 80 percent was determined by considering the structures of the USB IC and connector. From the verification solver, the maximum separation was 0.893 mm between the two lines, with a coupling rate of 76.6 percent. Referring to Table 1, the criteria were not satisfied. However, the ground shield ratio, which shows the extent the audio lines are shielded by a ground plane, does meet the specification of greater than 80 percent. These results are useful for verifying the layout of the audio lines.

Figure 4 shows the characteristics of the USB data lines (D+/D-) and memory bus lines, studied using the SI solver in PollEx. For the
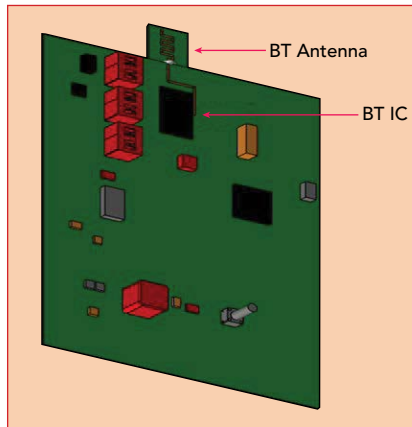
▲ Fig. 5 PCB surface thermal contours with natural convection (a) and forced air (b).

▲ Fig. 6 |S$_{11}$| of the MLA designed for BT.

▲ Fig. 7 MLA integrated with the BT PCB.

▲ Fig. 8 |S$_{11}$| of the MLA integrated with the PCB.

USB study, the ideal digital signal transmitted from the USB IC and received at the USB connector has a pulse width of 2.08 nS, corresponding to a data rate of 480 Mbps, with a peak voltage of 0.4 V. In Figure 4a, the received signals show enough voltage margin for normal USB operation because both the high threshold (0.3 V) and low threshold (0.1 V) USB 2.0 specifications are satisfied.[6] Similarly, the memory interface lines between the controller and the pseudo-static random access memory were analyzed (see Figure 4b). For this analysis, one differential clock line and a group of address lines were selected from the PCB design. The controller was assumed to send the clock signal with a frequency of 133 MHz and the address signals at a data rate of 256 Mbps. The eye diagram was simulated at the memory ports. The clock signal is used as a criterion to estimate the interface with the eye mask, whose high and low thresholds are 1.3 and 0.4 V, respectively. Additionally, it is assumed that the required setup and hold times for the interface are 2 and 1.5 ns, respectively. As the eye diagram shows sufficient voltage margin, the interface lines are well routed for reliable 256 Mbps data exchange between the controller and memory.

A board thermal analysis was performed to check the main audio amplifier's operating temperature, using the amplifier's quad flat package and 5 W power rating at room temperature. *Figure 5* shows the temperature contours for two conditions: 1) natural convection (see Figure 5a) and 2) forced air convection with an air flow of 5 m/s (see Figure 5b). With natural convection, the highest temperature of 85°C is the maxim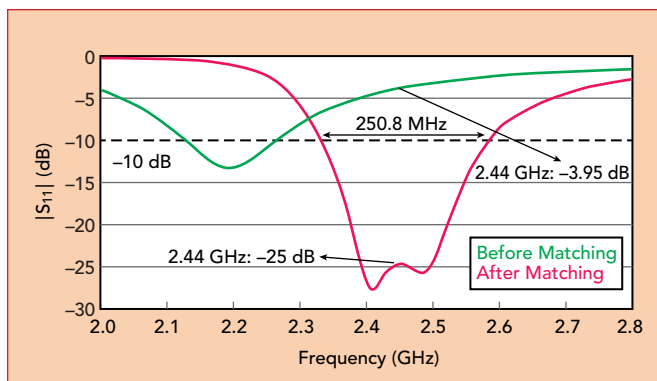um allowed for normal amplifier operation. Forced convection decreased the temperature from 85°C to 59°C, which improves reliability.
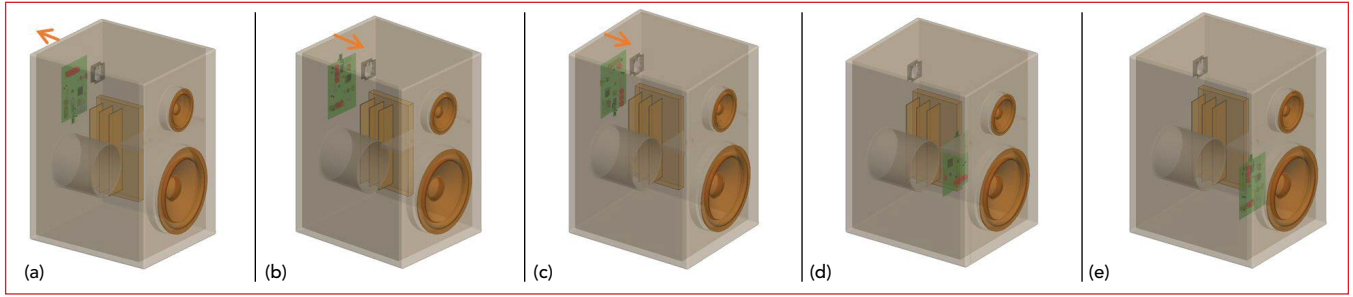
ANTENNA DESIGN AND INTEGRATION

The antenna design was inspired from the meander line antenna (MLA) concept proposed by Rashed and Tai.[7] The antenna was integrated on the PCB and placed in its working environment within the speaker assembly to identify the optimal location. Antenna electromagnetic (EM) characteristics in different configurations changing the location and orientation of the PCB inside the speaker cabinet were simulated using the 3D high frequency EM simulation tool, Altair Feko.[8]

Meandering the antenna increases the surface current path and enables reducing the antenna size. The resonant frequency of an MLA is a function of the meander separation and meander spacing; the resonant frequency can be reduced by increasing the meander separation, and vice versa.[9] As shown in *Figure 6*, the simulation showed the magnitude of the reflection coefficient of the MLA design on an FR4 substrate was approximately -17 dB at 2.4 GHz. The MLA integrated on the BT PCB is shown in *Figure 7*. The components on the PCB surrounding the antenna alter its resonance characteristics significantly (see *Figure 8*), requiring a matching circuit to restore the performance. The matching circuit comprises a simple LC network with a 0.778 pF series capacitor and a 53 nH shunt inductor, which shifts the resonance back into the BT frequency range.

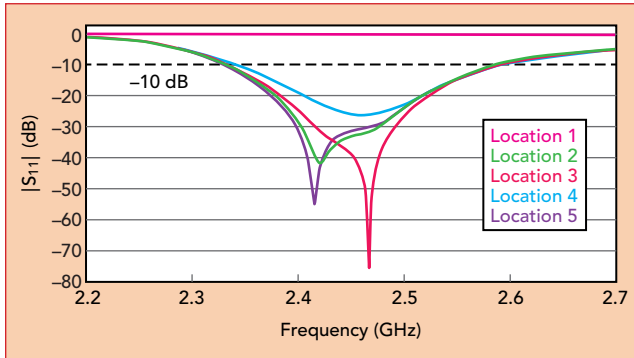The speaker cabinet is made of balsa wood with a dielectric constant of 1.3 and dimensions of 355 × 305

▲ Fig. 9 Antenna locations within the speaker cabinet: 1 (a), 2 (b), 3 (c), 4 (d) and 5 (e).

× 450 mm. In addition to the PCB, the components inside the speaker include a cooling fan, metallic heat exchanger, acoustic port and the speaker module. The location and orientation of the PCB are influenced by the spacing inside the cabinet, mounting support options and thermal efficiency. Taking these into account with the physical constraints, a complete in-situ analysis of the speaker assembly was performed considering several locations and orientations (see *Figure 9*). Location 1 places the antenna near the back wall of the speaker facing outward, i.e., toward the back side. Locations 2 and 3 mount the PCB on the same back wall facing inward, with the antenna pointed up and down, respectively. Locations 4 and 5 mount the PCB in free space between the components, facing inward and close to the back and front walls, respectively. Comparing the five positions, the magnitude of the reflection coefficient is less than -10 dB for all the locations except 1 (see *Figure 10*). The 3D radiation patterns (see *Figure 11*) show that locations 2 and 3 have nearly omnidirectional coverage along the horizon, which is required for good BT performance. Location 2 was chosen for the next step of the analysis, evaluating BT wireless coverage and the speaker's coexistence with Wi-Fi.

▲ Fig. 10 MLA $|S_{11}|$ for locations 1 to 5.

WIRELESS COVERAGE AND INTERFERENCE

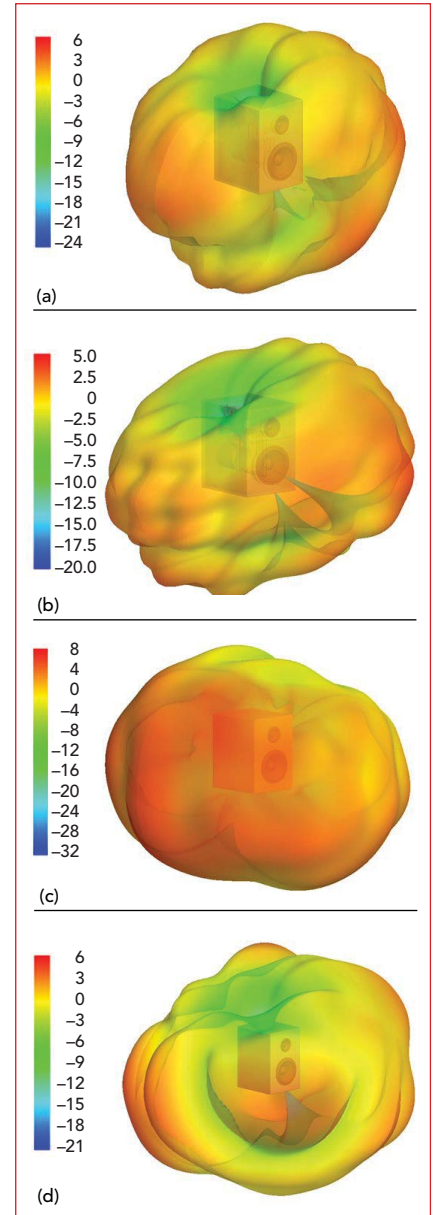With the advent of 5G and IoT, the trend is toward smart household electronics, including speakers. These smart devices use standards such as Wi-Fi, BT, LTE and ZigBee for connectivity, and some of these technologies operate in closely separated frequency bands, which can cause interference.[10] BT and Wi-Fi, for example, operate around 2.4 GHz and coexist, although interference from BT can reduce Wi-Fi throughput and vice versa. Analyzing interference through virtual prototyping early in the design stage can avoid costly rework later.
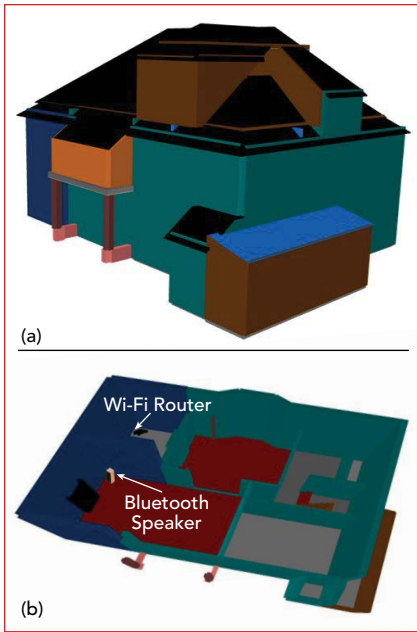
The effect of interference from Wi-Fi on the BT speaker was evaluated inside a multi-story residential building using Altair's wireless propagation and radio network planning software, WinProp.[8] For accurate analysis, the residential building model was detailed, comprising the multi-story design with thick walls, flooring, staircase, fireplace, cabinets, doors, windows and roof (see *Figure 12*). The BT speaker was placed in one corner of the living room and the Wi-Fi router in the corner of an adjacent room (see Figure 12b). The speaker was assumed to use the latest BT5 technology[11] and the Wi-Fi router the 802.11n standard.[12]

The BT speaker has near omnidirectional coverage along the horizon, as shown in Figure 11a. BT is a packet-based protocol with a master/slave architecture, one master can communicate with up to seven slaves in a pi-

▲ Fig. 11 3D radiation patterns showing the total realized gain (dBi) for locations 2 (a), 3 (b), 4 (c) and 5 (d).

conet. For this CDMA-based technology, the maximum number of codes available for a user on one carrier is seven. As BT supports a maximum data rate of 3 Mbps for the uplink (UL) and downlink (DL) through the en-

▲ Fig. 12 Multi-story house (a) and cross-section (b) showing the locations of the router and BT speaker.

hanced data rate transmission mode, the maximum achievable throughput should be 21 Mbps. Due to non-ideal orthogonality among the codes, however, the maximum achievable DL throughput is 19 Mbps (see *Figure 13*).

As 802.11n supports MIMO systems, a router with two antennas was used for the analysis, where each antenna carries one data stream in a 2 × 2 MIMO scenario. The router antennas are well matched for the 2.4 GHz Wi-Fi bands (see *Figure 14a*). For MIMO, the antennas must be well matched at the carrier frequency and well isolated to avoid interstream interference. Figure 14a shows the two antennas have good isolation, approximately ~25 dB. A better indication of independent behavior is the envelope correlation coefficient (ECC), shown in *Figure 14b*. For MIMO applications, an ECC value of 0.5 is considered okay, higher than 0.5 is considered bad and 0.3 or less is good. Being an orthogonal frequency-division multiplexing technology, 802.11n uses time-division duplex separation. The maximum achievable throughput is, therefore, the maximum achievable data rate. *Figure 15* shows the Wi-Fi access point in the modeled location provides good coverage for most of the house.
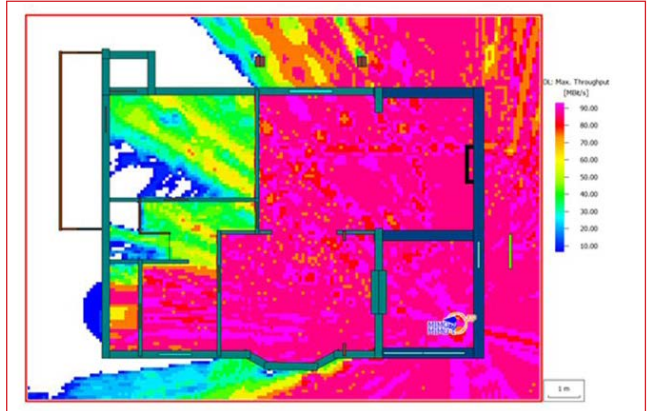
The Wi-Fi router operates on a 2412 MHz carrier, with the BT at 2442 MHz. The two are close to each other both in frequency and physically in the house. This leads to a decrease in BT throughput due to leakage from Wi-Fi into the BT frequency band, especially in the areas close to the Wi-Fi router (see *Figure 16a*). The interference from Wi-Fi to BT can be mitigated with additional filtering in the BT module. When the leakage from Wi-Fi causing the interference is attenuated by an additional 20 dB, the throughput is improved, as shown in *Figure 16b*.
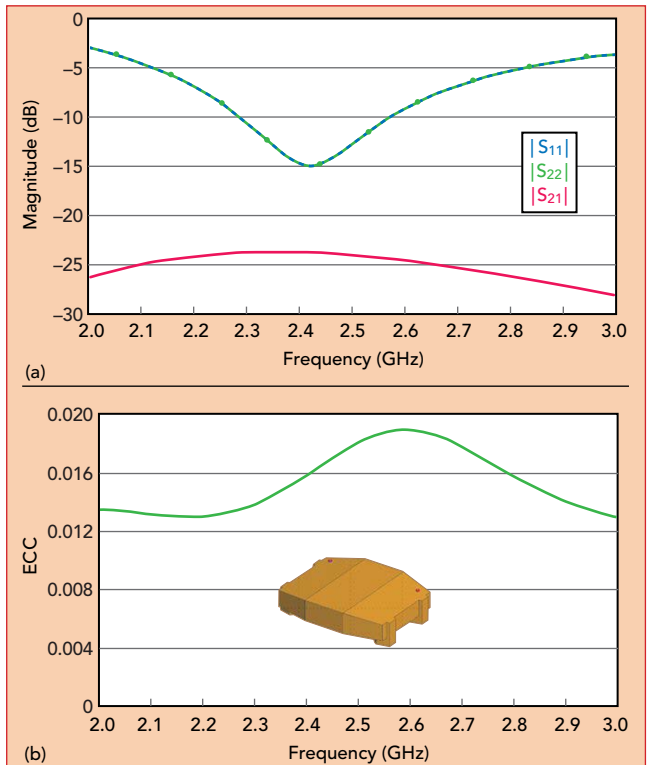
CONCLUSION

Simulation-driven virtual prototyping used during a smart product's development will reduce development time and ensure the design qualities of the product. These techniques were illustrated in three development stages of a wireless speaker: 1) PCB layout, 2) antenna design and integration and 3) wireless coverage and interference evaluation. Simulation-driven virtual prototyping results in smart products that are more cost-effective and provide higher quality and reliability.∎

▲ Fig. 13 Maximum achievable DL throughput for the BT speaker.

▲ Fig. 15 Maximum achievable Wi-Fi throughput using 802.11n, showing good coverage throughout most of the house.

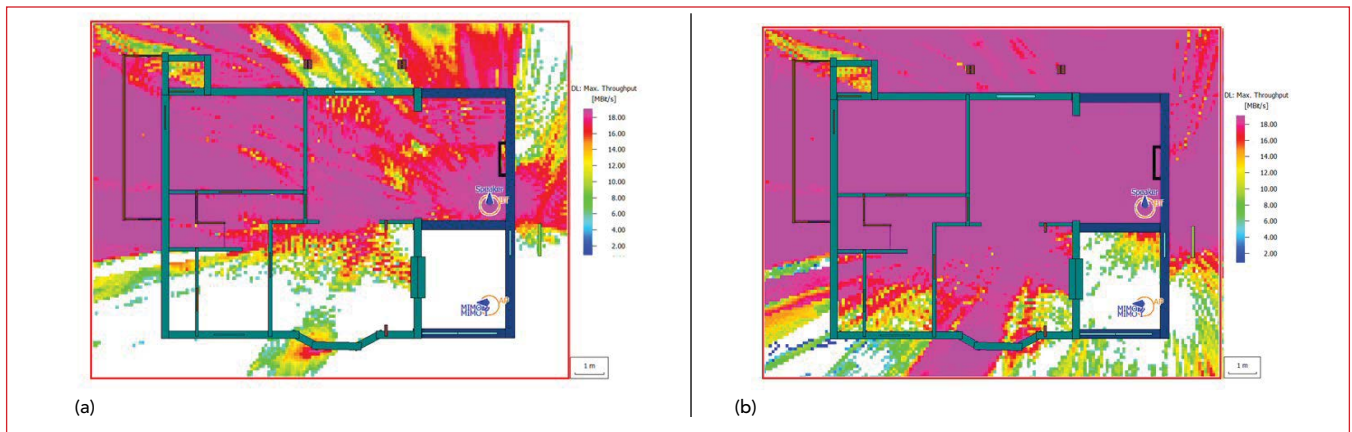▲ Fig. 14 Wi-Fi router antenna matching and isolation (a) and ECC (b).

▲ **Fig. 16** Effect of Wi-Fi interference on BT throughput: The white area near the Wi-Fi router indicates little BT coverage (a). Coverage can be improved with filtering to attenuate Wi-Fi leakage (b).

References

1. "5G Innovations for New Business Opportunities," *5G-PPP*, https://5g-ppp.eu/wp-content/uploads/2017/01/5GPPP-brochure-MWC17.pdf.
2. U. Sellgren, *Simulation-Driven Design – Motives, Means and Opportunities*, Doctoral Thesis, The Royal Institute of Technology, 1999.
3. S. Koziel, X. S. Yang and Q. J. Zhang, *Simulation-Driven Design Optimization and Modeling for Microwave Engineering*, Imperial College Press, London, 2013.
4. G. G. Wang, "Definition and Review of Virtual Prototyping," *ASME Journal of Computing and Information Science in Engineering*, Vol. 2, No. 3, September 2002, pp. 232-236.
5. Altair PollEx, www.altair.com/pollex/.
6. "Universal Serial Bus Specification Revision 2.0," April 2000, http://sdpha2.ucsd.edu/Lab_Equip_Manuals/usb_20.pdf.
7. J. Rashed and C. T. Tai, "A New Class of Resonant Antennas," *IEEE Transactions on Antennas and Propagation*, Vol. 39, September 1991, pp. 1428-1430.
8. Altair Feko, www.altair.com/feko/.
9. S. R. Best and J. D. Morrow, "Limitations of Inductive Circuit Model Representations of Meander Line Antennas," *IEEE Antennas and Propagation Society International Symposium*, June 2003.
10. U. Wetzker, I. Splitt, M. Zimmerling, C. A. Boano and K. Römer, "Troubleshooting Wireless Coexistence Problems in the Industrial Internet of Things," *IEEE International Conference on Computational Science and Engineering*, August 2016.
11. "Bluetooth Core Specification Version 5.0 Overview," *Bluetooth SIG*, www.bluetooth.com/bluetooth-resources/bluetooth-5-go-faster-go-further/.
12. "IEEE 802.11n-2009 – IEEE Standard for Information technology--Local and Metropolitan Area Networks--Specific requirements--Part 11: Wireless LAN Medium Access Control (MAC) and Physical Layer (PHY) Specifications Amendment 5: Enhancements for Higher Throughput," *IEEE Standards Association*, October 2009, https://standards.ieee.org/standard/802_11n-2009.html.